Study of the binding interaction between fluorinated matrix metalloproteinase inhibitors and Human Serum Albumin

ARTICLE *in* EUROPEAN JOURNAL OF MEDICINAL CHEMISTRY · MARCH 2014

Impact Factor: 3.45 · DOI: 10.1016/j.ejmech.2014.03.064 · Source: PubMed

9 AUTHORS, INCLUDING:

Claudio Cassino
Amedeo Avogadro University of Eastern Pie…
30 PUBLICATIONS **655** CITATIONS
SEE PROFILE

Carlos F G C Geraldes
University of Coimbra
182 PUBLICATIONS **3,396** CITATIONS
SEE PROFILE

Alessandro Maiocchi
Bracco Group
32 PUBLICATIONS **673** CITATIONS
SEE PROFILE

Armando Rossello
Università di Pisa
131 PUBLICATIONS **1,148** CITATIONS
SEE PROFILE

Study of the binding interaction between fluorinated Matrix Metalloproteinase inhibitors and Human Serum Albumin

Giuseppe Digilio[1*], Tiziano Tuccinardi[2], Francesca Casalini[1,2], Claudio Cassino[1], David M. Dias[3,4,5], Carlos F.G.C. Geraldes[3,4,6], Valeria Catanzaro[1,7], Alessandro Maiocchi[8], Armando Rossello[2]

[1] Department of Science and Technological Innovation, Università del Piemonte Orientale "Amedeo Avogadro", Viale T. Michel 11, I-15121 Alessandria, Italy;

[2] Department of Pharmacy, University of Pisa, Via Bonanno 6, I-56126 Pisa, Italy;

[3] Center for Neurosciences and Cell Biology of Coimbra, Coimbra, Portugal;

[4] Department of Life Sciences, Faculty of Science and Technology University of Coimbra, Coimbra, Portugal;

[5] Present address: Chemistry Department, University of Cambridge, Cambridge, United Kingdom;

[6] Coimbra Chemistry Centre, University of Coimbra, Coimbra, Portugal.

[7] Istituto di Ricerca Diagnostica e Nucleare SDN, Via Gianturco 113, Napoli, 80143, Italy.

[8] CRB Bracco Imaging SpA, Via Ribes 5, I-10010 Colleretto Giacosa (TO), Italy.

* Corresponding author:
Dr. Giuseppe Digilio
Department of Science and Technological Innovation, Università del Piemonte Orientale "Amedeo Avogadro", Viale T. Michel 11, I-15121 - Alessandria (AL), Italy.
Voice: + 39 0131 360371
Fax: + 39 0131 360250
email: giuseppe.digilio@mfn.unipmn.it

Abstract

Fluorinated, arylsulfone-based inhibitors of Matrix Metalloproteinases (MMP) have been used, in the [^{18}F]-radiolabelled version, as radiotracers targeted to MMP-2/9 for Positron Emission Tomography (PET). Although they showed acceptable tumor uptake, specificity was rather low. To get further insights into the reason of low specificity, the binding interaction of these compounds with Human Serum Albumin (HSA) has been investigated. ^{19}F-NMR spectroscopy showed that all compounds considered partition between multiple HSA binding sites, being characterized by either slow-exchange kinetics (with K_a in the order of 10^5 M^{-1}) and fast-exchange kinetics (with K_a in the order of 10^4 M^{-1}). For 2-(2-(4'-(2-fluoroethoxy)biphenyl-4-ylsulfonyl)phenyl)acetic acid (**1a**) and 2-(2-(4'-(2-fluoroacetamido)biphenyl-4-ylsulfonyl)phenyl)acetic acid (**1c**), these slow and fast-exchanging binding sites could be mapped to Sudlow's site I and II, respectively. It is shown that high affinity albumin binding constitutes a theoretical limitation for the specificity achievable by MMP-inhibitors as MMP-targeted PET tracers in cancer imaging, because albumin accumulating aspecifically in tumors lowers the binding potential of radiotracers.

Keywords

Albumin; Fluorine; Matrix Metalloproteinase inhibitor; binding affinity; ^{19}F-NMR; Saturation Transfer Difference; molecular dynamics.

List of abbreviations

MMP: matrix metalloproteinases; HSA: human serum albumin; ECM : extracellular matrix ; TIMP: tissue inhibitor of metalloproteinase; MMPi: inhibitor of matrix metalloproteinase; ZBG: zinc binding group; PEG: polyethylene glycol; STD NMR: saturation transfer difference NMR; GEM: group epitope mapping; PLR: protein-to-ligand ratio; SNR: signal-to-noise ratio; MD: molecular dynamics; MM-PBSA: Molecular Mechanics - Poisson Bolzmann Surface Area.

Introduction

Matrix Metalloproteinases (MMPs) are a family counting more than 25 members of calcium- and zinc-dependent endoproteases that are secreted in the extracellular matrix (ECM) or displayed on the extracellular side of the plasma membrane.[1,2] Although the primary role of MMPs is the degradation of specific structural components of the ECM, such as the different types of fibrillar collagen (the preferred substrate of MMP-1/8/13/18), non-fibrillar collagen (MMP-2/9) and proteoglycans (MMP-3/7/10),[3] they are known to have additional regulatory functions, including the processing of chemokines, cytokines, growth-factors, and even other MMPs and their tissue inhibitors (TIMPs).[4,5] The diverse roles of MMPs in the regulation of tissue microenvironment and in the remodelling of the ECM have been soon recognized to be of high relevance for cancer biology, as high levels of MMPs, most notably the gelatinases (MMP-2 and MMP-9), have shown positive correlation with cancer invasiveness and malignancy.[6,7] Therefore, the MMP activity profile can be regarded to as kind of signature of the staging and invasiveness of a tumor.

Because of their extracellular localization, MMPs have been long taken into consideration as targets for anti-cancer therapy and large libraries of low molecular weight compounds as highly potent, broad-spectrum MMP inhibitors (MMPi) are nowadays available.[8,9] Such MMP inhibitors are based on compounds that insert through a hydrophobic portion into the enzyme S_1' specificity pocket and chelate the catalytic zinc ion through a suitable zinc binding group (ZBG), often represented by hydroxamate. Besides a therapeutic target, MMPs also appeared as valuable targets to grade cancers by means of a variety of imaging techniques.[10,11,12,13,14] To obtain MMP targeted tracers for nuclear medicine, a number of MMPi initially developed for therapy have been radiolabelled with γ-emitting or β^+-emitting nuclides. Several radiolabelled versions of hydroxamate-based MMPi as tracers for PET/SPECT have been described.[15,16,17,18] However, concerns have been raised with hydroxamate-based radiotracers, essentially linked to the metabolic stability of hydroxamate and to the lack of selectivity for those members of the MMP family that are more descriptive of a disease. Hence, many efforts have been directed to non-hydroxamate, selective radiolabelled tracers.[19,20] ùù

We have recently proposed fluorinated arylsulfone MMPi with carboxylate as the ZBG as potential tracers for imaging gelatinases by PET. These compounds were derived by modification of precursor **A**, first described in ref 21, to allow for the insertion of a fluorine atom (Scheme 1).[22] Amongst these fluorinated MMPi, compound **1a** showed the best MMP affinity profile, being endowed with nanomolar affinity for MMP-2/9/12/13 and a marked selectivity over MMP-1/3/14. Preliminary studies with a heterotopic human U-87 MG glioblastoma mouse model showed a detectable tumor uptake of the radiolabelled version of **1a** (*i.e.* tracer **[^{18}F]-1a**), with a preferential accumulation of the radioactivity within the active periphery as compared to the necrotic tumor

core. Accumulation of radioactivity in the tumor rim was found to co-localize with the gelatinase activity, but the specificity of uptake of the tracer in the tumor rim was only 18%. A major contribution to the aspecific localization of radioactivity within the tumor rim has been related to the high affinity of **[^{18}F]-1a** for serum albumin. Serum albumin is the most abundant protein in serum plasma (reaching a concentration of 35 mg/mL in mice) and is capable to bind a wide range of endogenous as well as exogenous compounds. The multi-domain structure of albumin accommodates multiple binding sites, some of which are known to have high affinity for small anionic aromatic compounds,[23,24,25] as compounds shown in Scheme 1 are.

The aim of the present work is to characterize at the molecular level the binding mode between our arylsulfone based MMPi and human serum albumin (HSA). To this regard, ^{1}H Saturation Transfer Difference NMR (STD-NMR) and ^{19}F-NMR studies have been combined with molecular dynamics/docking calculations to assess ligand binding affinities and binding epitopes within the albumin binding sites. This piece of information is critical to the rational design of modified [^{18}F]-radiolabelled arylsulfones as MMP-targeted PET tracers endowed with minimized affinity for serum albumin.

Results

Interaction with serum albumin by ^{19}F-NMR

The binding modes of the fluorinated compounds with human serum albumin (HSA) have been assessed by ^{19}F-NMR titration of the inhibitors with HSA. All ligands considered, in the absence of albumin, show a single ^{19}F-NMR signal with linewidth (proton decoupled) of about 2 Hz (Figure 1). In the presence of albumin, the linewidth increases (up to 200-220 Hz) and multiple ^{19}F-NMR resonances appears in the presence of intermediate to high albumin concentration, whose number and spectral features varied from ligand to ligand.

The ^{19}F-NMR signal of **1a** (marked as signal A in Figure 1) shows a progressive downfield shift with line-broadening with increasing albumin concentration. In addition, at intermediate protein-to-ligand ratio (PLR=0.65:1) a new broad ^{19}F-NMR signal (signal B) emerges from the noise 1.46 ppm (corresponding to 690 Hz) downfield the resonance of the free ligand. Signal B becomes increasingly intense relative to signal A as the PLR increases further. At a PLR of 2.9:1, where albumin binding sites exceed the ligand concentration, the area under signal B becomes larger than that of signal A (area ratio 2:1), while their linewidths are comparable (about 200-220 Hz). This can be explained by considering at least two different types of binding sites on albumin: type-A and type-B sites. Type-A sites are endowed with fast exchange kinetics on the ^{19}F-NMR timescale, such

that the chemical shift (and linewidth) of the corresponding signal (signal A) appears as the weighted average between that of the free form and that of the bound form of the ligand. Type-B sites are endowed with slow exchange kinetics, such that the fluorinated ligand bound in that site yields a signal with constant chemical shift and large linewidth (about 200 Hz) all throughout the titration (signal B). According to the ^{19}F-NMR timescale for slow exchange (k_{ex}<<$\delta\nu$), molecules specifically bound to type-B sites show k_{ex}<<690 Hz. It is worth noting that ^{19}F-NMR titrations were done with incremental number of scans on going from the first point of the titration (no albumin, number of averages = 128) to the last point (PLR 2.9:1, number of scans = 16K). This experimental setup was chosen to compensate for the effect of decreasing signal-to-noise ratio (SNR) with increasing ^{19}F-NMR linewidths along the titration. Therefore, signal B becomes detectable when the concentration of occupied type-B sites becomes sufficiently high (this happens at about 0.65 mM albumin concentration, Figure 1), while in the initial points of the titration signal B does not emerge from the baseline because of insufficient SNR. Therefore, ligand **1a** can be thought to partition between slow- and fast-exchanging binding sites. After the equivalence point (*i.e.* PLR> 0.5, assuming two binding sites per albumin molecule), the area under signal B increases over that of signal A with increasing PLR, indicating that in conditions approaching excess binding sites the ligand has a preference for the slow-exchanging type-B site as compared to the fast-exchanging type-A sites.

Competition ^{19}F-NMR experiments were performed to identify which albumin binding sites were specifically involved in ligand binding, focussing the attention to Sudlow's site I (large binding site located on subdomain IIA) and site II (smaller binding pocket located on subdomain IIIA).[23,26,27] Competition experiments were done with warfarin (a well-known site I ligand) and ibuprofen (a site II ligand, but having non-negligible binding also to other sites).[23] Warfarin added at 1.0 mM final concentration to a solution of HSA (2.0 mM) and **1a** (1.0 mM) causes a decrease of the intensity of signal B relative to signal A, while at 16.0 mM warfarin concentration signal B completely disappears and signal A is slightly shifted upfield (Figure 2). Thus, warfarin is able to displace **1a** from site-B and to make it available for the binding equilibrium with site-A. Ibuprofen at 1.0 mM final concentration does not appreciably affect the ^{19}F-NMR spectrum of the HSA/**1a** mixture, while at 16.0 mM it causes the disappearance of signal B and a slight upfield shift of signal A. These observations are consistent with the assignment of signal B to **1a** occupying the warfarin site (Sudlow site I), while signal A can be assigned to **1a** within the ibuprofen site (Sudlow site II). However, additional contributions to signal A due to **1a** bound to secondary sites (*e.g.* lower affinity sites other than Sudlow's site I or II) can not be excluded. Ibuprofen at high concentration can displace **1a** both from site I and site II, because ibuprofen is well-known to have a secondary

albumin binding site partially overlapping with that of warfarin, as well as to modify binding affinities to other sites through allosteric effects.[28] It is worth noting that in the presence of warfarin a new binding site for **1a** appears (broad ^{19}F-NMR signal at -148.6 ppm, Figure 2), which was not observed in the absence of warfarin. Such a site is likely arising from allosteric-like modulation resulting from co-binding of the ligand and warfarin, or by the interaction of warfarin and **1a** within partially overlapping binding sites.

Compound **1c** behaves very similar to **1a**, distributing between a slow-exchanging B-type site (signal B, 2.5 ppm or 1175 Hz downfield relative to the free ligand) and fast-exchanging A-type sites (signal A, Figure 1). At a PLR $\geq$ 1.30, the ligand appears to be completely bound to albumin and signal B increases at the expenses of signal A, indicating a higher affinity for the former site. As for **1a**, displacement experiments with either warfarin or ibuprofen allowed us to assign signal B and signal A to **1c** being bound at Sudlow's site I and II, respectively (Figure 2).

For compound **2**, signal B (slow exchange on the ^{19}F-NMR timescale) appeared 2.0 ppm (810 Hz) upfield relative to the resonance of the free ligand, and its intensity rapidly increased at the expenses of signal A with increasing PLR. At a PLR of 1.15, signal A vanished while signal B reached the maximum intensity. With increasing PLR, (*i.e.* in conditions where the concentration of each binding site exceeds the total ligand concentration) the ligand appears essentially bound to slow-exchanging site(s), making the ligand no more available to A-type sites. Thus, B-type sites have a substantially higher affinity for **2** than A-type sites. Displacement experiments indicate that warfarin (16 mM final concentration) is a very weak displacer of **2**, while ibuprofen (16 mM final concentration) is much more effective. Ibuprofen can clearly displace the ligand from site-B making it available to site-A and likely to other secondary binding sites. However, in the presence of ibuprofen, a new peak appears at -45 ppm (very close to the type-B peak), indicating that binding of ibuprofen either opens a new binding site for **2** or modifies an existing site by co-operation or allosteric effects. The assignment of the ^{19}F-NMR signals of ligand **2** to specific binding sites still remains ambiguous.

Finally, compound **1b** shows the most complex distribution of binding modes, with at least four different modes giving rise to separate signals (A, B, B' and B''). By analogy with the other ligands, signals B and B' appear to be related with sites having slow exchange kinetics, and may represent binding modes with higher affinity. Due to the high complexity of this system, no displacement experiments were performed to further characterize the binding sites.

Assessment of association constants

^{19}F-NMR titration data for **1a/1c/2** could be analyzed to extract association constants K_a^B and K_a^A for ligand binding to slow exchanging (B-type) and fast-exchanging (A-type) sites, respectively, according to a model based on the following approximations: *i)* binding sites are independent (binding to one site does not affect binding to other sites); *ii)* affinity constants are large enough, such that at relatively high PLR (when the total number of binding sites is larger than the total ligand concentration) the concentration of the free ligand becomes negligible as compared to that of the bound ligand); *iii)* fast-exchanging sites, if more than one, are all equivalent (*i.e.* they have the same binding constant). The association constants can be then evaluated with a two-step procedure. First, the full binding isotherms obtained by plotting ^{19}F-NMR chemical shift of signal A versus the total albumin concentration HSA_T (Figure 3) are considered. The association constants for A-type sites can be obtained by fitting such isotherms according to the model described in ref. 29, modified to account for the fact that ligand binding to site-B (slow exchange, higher affinity site) lowers the concentration of the free ligand [*L*] available to interact with site-A (see supporting information for details about this model). By this procedure an estimation of K_a^A (and the number of equivalent A-type binding sites, n_A) can be obtained (Table 1). Second, the ratio $K=K_a^A/K_a^B$ between the association constants for binding to site-A and site-B can be obtained by considering the change of the molar ratio of the ligand bound at site-A ($[AL]/[L]_T$, or χ^A) as a function of $[HSA]_T$, considering only data points at high PLR (*i.e.* beyond the equivalence). At high PLRs, the concentration of the free ligand $[L]_F$ can be assumed to be negligible with respect to the total ligand concentration $[L]_T$ (*i.e.* $[L]_T = [AL] + [BL]$, with [*AL*] and [*BL*] being the concentration of the site-A bound ligand and the site-B bound ligand, respectively; see supporting info for details about the model). According to this approximation, χ^A *vs* $[HSA]_T$ titration data of our ligands could be fit to yield K_a^A/K_a^B = 0.09, 0.14 and 0.03 for **1a**, **1c** and **2**, respectively (Table 1). Because of the complexity of the ^{19}F-NMR spectrum of **1b**, no attempts have been made to analyze binding isotherms. Finally, an estimation of K_a^B was eventually achieved by combining K_a^A with the K_a^A/K_a^B ratio. The results indicate that K_a^B are in the order of 10^5 M^{-1} (with **2** having the highest affinity), while K_a^A are in the order of 10^4 M^{-1}, with multiple low affinity binding sites being available for **1c** and **2** (Table 1). Along all these calculations, only one high affinity binding B-type site per albumin molecule was allowed. The order of magnitude of the binding constants thus obtained is well-consistent with those of a number of low molecular weight ligands with anionic character.[27]

Saturation Transfer Difference - NMR

The interaction between arylsulfones and albumin was further investigated by ligand-based NMR methods, namely by means of STD-NMR. This is one of the most informative and robust techniques available for detecting molecular interactions and define the ligand epitopes making the closest contacts within the protein residues of the binding pockets.[30] When proteins are pre-irradiated at a frequency centred on the aliphatic protein protons (0 ppm), saturation spreads out to the whole protein proton ensemble through spin diffusion, and eventually to the protons of the ligand making the closest contacts with the protein spin reservoir. The extent of protein-to-ligand saturation transfer can be quantitatively measured on a proton-by-proton basis in terms of saturation transfer amplification factors (A_{STD}), whose values reflect the distance between the ligand and protein protons, and therefore provide information on the conformation of the ligand bound state.[31]

For all compound tested in this work, all the ligand ^{1}H NMR resonances contribute to the STD-NMR spectra obtained (see Figure S2-S5), indicating a tight interaction between the ligands and the protein as found within the ^{19}F-NMR study. To have a better picture of which part of the ligands established the closest contacts with proteins residues, a group epitope mapping (GEM) characterization was performed (Table 2). Differences are found in the profile of A_{STD} values amongst the biphenyl-type (**1a/1b/1c**) and the phenoxy-type arylsulfones (**2**). The former ligands share a common epitope for their interaction with HSA, showing maximum A_{STD} values (normalized as GEM%) for the protons H_c and H_d of the phenylacetic acid moiety (Figure 4) and lower (but still high) GEM% values for the protons belonging to the biphenyl ring. In contrast, compound **2** gives the largest GEM% at the level of the *p*-fluoro-phenoxy ring, while GEM% steadily decreases on going from such moiety to the opposite edge (*i.e.* the phenylacetic acid moiety) of the molecule. This clearly indicates that the binding topology of **2** is different from that of **1a/1b/1c**. It must be emphasized that such epitopes were obtained in conditions of large excess of the ligand (1.0 mM) with respect to albumin (0.03 mM), such that ligands are predicted, on the basis of ^{19}F-NMR data, to be populating multiple binding sites (either specific and aspecific). As a result, STD amplification factors and GEM percentages reflect contributions from each binding mode rather than describing a single binding mode.

Modelling of inhibitor binding to human serum albumin

In order to suggest a possible binding mode for the carboxylate-based arylsulfone MMP inhibitors, the interaction of compound **1a** was deeply analyzed by means of docking and molecular dynamic (MD) simulations. The crystallographic structure of warfarin (2BXD PDB code) and diazepam, (2BXF PDB code)[23] complexed with human serum albumin were used for analysing the binding

interaction of **1a** into Sudlow's site-I and site-II, respectively. Compound **1a** was docked into the two possible binding sites using seven different docking procedures, resulting in a total of 140 different poses collected for each binding site. These docking poses were clusterized on the basis of their superimposition inside the binding site. Twelve clusters were so obtained for the interaction of **1a** into site-I, whereas fifteen different binding poses were postulated for site-II. A representative docking pose of each of these 27 clusters was then subjected to MD simulations. The HSA-ligand complexes were used as starting points for 10 ns of MD with explicit water molecules, as described in the Experimental section. The 27 MD trajectories obtained in this way were further analyzed through the Molecular Mechanics - Poisson Bolzmann Surface Area (MM-PBSA) method[32] that has been shown to accurately estimate the ligand–receptor energy interaction.[33,34] This approach averages the contributions of gas phase energies, solvation free energies, and solute entropies calculated for snapshots of the complex molecule as well as the unbound components, extracted from MD trajectories, according to the procedure fully described in the Experimental section. With regards to site-II, the MM-PBSA results (Table 3) suggest that there is one docking pose that is the most favorable, as it shows an interaction energy ΔPBSA = -33.5 kcal•mol^{-1}, more than 13 kcal•mol^{-1} higher than all the other binding poses (docking pose 18, Table 3). Figure 5 shows the energy minimized average structures of the last 7 ns of HSA complexed with the hypothesized binding pose (pose 15, Table 3) of compound **1a** in the site-II. The overall conformation of the ligand is similar to that observed for this class of compounds into the MMP binding site.[21]

The carboxylic function of the compound shows a strong ionic interaction with R434 and an H-bond with N415 and Y435. The sulfonyl group forms an H-bond with R509 and the phenylacetic ring shows important lipophilic interactions with the side chain of I412, L454, L457 and L477. With regards to the biphenyl portion, it is highly exposed to the solvent and shows a lipophilic interaction with L411 and a cation-π interaction with R434. The comparison between the binding pose of **1a** and ibuprofen in site-II (2BXG PDB code) highlights a common binding mode. As shown in Figure 5, the phenylacetic portion of **1a** shows the same disposition of the (S)-2-phenylpropionic acid portion of ibuprofen. With regards to site-I, there is one pose that shows a very high interaction energy (pose 10, see Table 3), that is about 16 kcal•mol^{-1} more stable than all the others. Figure 6 shows the energy minimized average structures of the last 7 ns of HSA complexed with the hypothesized binding pose 10 of compound **1a** in the site-I. The carboxylic function of the compound shows a strong ionic interactions with R246. The sulfonyl group forms an H-bond with K223 and H266 and the phenylacetic ring shows lipophilic interactions with L262. With regards to the biphenyl portion it shows a lipophilic interaction with Y174; furthermore, the oxygen atom of the 2-fluoroethoxy fragment shows an H-bond with S216. The comparison between

the binding pose of **1a** and warfarin in site-I (2BXD PDB code) highlights a completely different binding mode for these two compounds (Figure 6). Finally, in order to compare the binding interaction energy of compound **1a** into site-I and site-II, for the best binding pose of **1a** into the two binding sites, solute entropy was evaluated and included in the interaction energy equation. As shown in Table 4, the interaction of **1a** into site-I is about 3 kcal•mol^{-1} higher that of **1a** into site-II, in an agreement with the experimental results that suggest a preferential interaction of the compound into site-I.

Discussion

Human serum albumin interacts reversibly with a broad spectrum of compounds, either endogenous or not. Low molecular weight compounds with moderately to high hydrophobicity or with amphiphilic character (including small anionic compounds) usually bind to one or very few high-affinity sites, with typical association constants in the range 10^4-10^6 M^{-1}.[27] The most characterized amongst these primary binding sites are Sudlow's site I, preferred by bulky heterocyclic anions, and Sudlow's site II, preferred by aromatic carboxylates with an extended conformation.[23] In addition to primary sites, several other secondary sites with lower or very low affinity exist. It was recognized early on that ^{19}F-NMR spectroscopy is a powerful tool to characterize the albumin binding of fluorinated ligands, and to study their distribution amongst primary and secondary binding sites. Fluorine containing ligands, such as as 5-F-L-triptophan, 5-F-salicylic acid, or the drug sulindac, were found to bind to albumin yielding one or multiple specifically shifted ^{19}F-NMR resonances, usually characterized by slow exchange kinetics on the ^{19}F-NMR timescale.[35,36,37] In addition to the specifically shifted signal, one fast-exchange averaged ^{19}F-NMR signal is typically found, due to binding equilibria with one (or multiple) secondary site. All the arylsulfones we studied behave along this line, as all of them interact with albumin through multiple binding sites and with different exchange kinetics. The unambiguous assignment of albumin-bound ^{19}F-NMR resonances of **1a** and **1c** has been obtained, showing high affinity binding at site I with K_a in the order of 10^5 M^{-1}. Furthermore, binding to site II and other secondary sites yielded significant affinity, in the order of 10^4 M^{-1} (Table 1). Modelling of the binding poses and energies of **1a** within Sudlow's site I and II gave interaction energies that follow the order of the experimental affinity constants.

^{19}F NMR experiments revealed the complexity of the interactions between albumin and arysulfone ligands, arising from binding to multiple primary sites and additional, rather undefined, non-specific sites. Because of simultaneous binding to such a variety of sites, STD amplification factors and GEM percentages have population-weighted contributions from each binding site. Therefore, GEM

percentages do not describe a single binding pose within a single binding site, but rather describe a global average of the interaction of molecular epitopes within all available binding sites. In this perspective, ^{1}H STD-NMR measurements revealed that arylsulfones make very tight interactions with protein residues within the binding pockets, and that all portions of the ligands (including the rather peripheric fluorine-bearing substituent of the biphenyl) contribute to define the binding pose and site preferences. This is confirmed by the finding that **1b**, although differing from **1a/1c** only for the biphenyl substituent, shows a very different distribution amongst the available binding sites. Also, the introduction of a bend within the biphenyl ring (resulting in the phenoxy-derivative **2**) has a substantial effect on the pattern of protein-ligand atomic interactions (as shown by ^{1}H STD-NMR) and on the preference for primary binding sites. Despite small changes in the arylsulfone structure have consequences on binding preferences and binding poses, the affinity for albumin remains very high.

This fact has a very large impact in regard to the application of the [^{18}F]-radiolabelled version of these compounds as MMP-specific tracers. In a previous study, compound **[^{18}F]-1a** was used as a PET tracer to specifically visualize MMP-2 within a U87 MG glioblastoma mouse model expressing high levels of MMP-2.[22] In that study, the accumulation of the tracer in the tumor was only 18% specific, while on theoretical grounds specificity was expected to be higher than 90% (corresponding to an experimentally determined binding potential B_{max}/K_d for MMP-2 of 14). High affinity for albumin can explain, at least partially, the reasons for such a low specificity. Assuming a concentration of albumin of 0.4 mM in the mouse blood, and given an association constant for albumin/ligand interaction of 10^5 M^{-1} (Table 1), it can be calculated that more than 99% of the **[^{18}F]-1a** tracer gets bound to albumin in the bloodstream (here only the binding within the highest affinity site is considered). Extravasation of the tracer/albumin complex into the tumor essentially occurs by the enhanced permeation and retention (EPR) effect, leading to the aspecific accumulation of the tracer/albumin complex within the tumor extracellular interstitium, or within tumor associated oedema. As a matter of fact, albumin is long known to accumulate in and be catabolized by tumors, and it has been exploited to enhance or image biodistribution of anti cancer drugs[38] as well as to assess, in the radioiodinated form, the tumor distribution space.[39] Compartimentalization of albumin-bound compounds within the perivascular space and tumor interstitium has been visualized through an elegant DCE-MRI approach. Pharmacokinetics modelling showed unidirectional transport from the extravascular to the perivascular space, leading to albumin pooling within the interstitium and slow tumor clearance by convection and/or the poorly efficient tumor lymphatics. [40]

Within the tumor interstitium, the tracer can be thought to distribute between the albumin binding sites and MMP-2 active sites according to the following equilibrium:

$$HSA-tracer+MMP \Leftrightarrow HSA+MMP-tracer$$

whose equilibrium constant is $K_{eq}=\frac{K_a^{MMP}}{K_a^{HSA}}$ (where K_a^{MMP} and K_a^{HSA} are the association constants for binding to MMP-2 and HSA, respectively). By considering that $[MMP]_{tot} >> [tracer]_{tot}$, as usual for radiotracers, the partitioning of the tracer between MMP-2 and albumin binding sites is described by:

$$\frac{[MMP-tracer]}{[HSA-tracer]}=\frac{K_a^{MMP}}{K_a^{HSA}}\frac{[MMP]_{tot}}{[HSA]_{tot}} \qquad \text{(eq. 1)}$$

where [*MMP-tracer*] and [*HSA-tracer*] represent the concentration of the ligand bound to MMP-2 or albumin, respectively. The [*MMP-tracer*]/[*HSA-tracer*] ratio takes the role of the binding potential in conditions where the fraction of tracer not bound to the target MMP is considered to be present as albumin-bound rather than as free ligand. The [*MMP-tracer*]/[*HSA-tracer*] ratio can be transformed into the binding specificity defined as:

Specificity % = 100 * [*MMP-tracer*] / ([*MMP-tracer*]+[*HSA-tracer*])

The concentration of active MMP-2 (*i.e.* $[MMP]_T$) in the glioblastoma tumor model has been estimated to be 200 nM, while the association constant (K_A^{MMP}) for the interaction between **1a** and MMP-2 is $6.7\text{x}10^7$ M^{-1}.[22] If only one, high affinity site on albumin is considered (site I with $K_a^{HSA}=1.0\text{x}10^5$ M^{-1}, see Table 1) and assuming a concentration of (extravasated) albumin of 0.4 mM, the [*MMP-tracer*]/[*HSA-tracer*] ratio can be rated at 0.33, corresponding to a specificity for MMP-2 labelling of 25%. This value is not too far from 18%, *i.e.* the value found by *in vivo* experiments. In terms of binding potential, the effect of albumin will lower the theoretical B_{max}/K_d to substantially less than 10, the value that is considered as a reasonable goal for planar imaging for tracers with nanomolar affinity.[41] It worth noting that, according to the model described by eq. 1, the binding specificity would increase to 64% if binding to specific sites (both site I and site II), but not aspecific binding, could be abolished. Of course, higher specificity can be achieved by lowering the dissociation constant for the interaction of the ligand with the target MMP. Thus, albumin binding constitutes a theoretical limitation for the specificity achievable by MMP-targeted tracers in cancer imaging. Interestingly enough, a number of tracers which were proposed as potential MMP tracers in cancer but were discontinued or gave disappointing results *in vivo* appear as good albumin binders, being hydrophobic aromatic anions (for instance, [^{18}F]-SAV03,[20] or the radioiodinated biphenyl sulfonamides described in ref. 42).

In addition to aspecific accumulation of albumin in the tumor interstitium, specific mechanisms of albumin uptake and catabolism shown by many tumors can also contribute to the accumulation of albumin-bound molecules within tumors. As a matter of fact, albumin has been exploited as a carrier to enhance the delivery of anti-cancer drugs such as paclitaxel within cancer cells through a mechanism involving the specific protein-protein interaction between albumin and the matricellular SPARC protein. [43,44,45]

The minimization of the affinity for albumin appears of paramount importance to enhance the specificity of MMP-2 PET tracers in cancer. Binding to albumin (and perhaps to other serum components) is largely linked to the hydrophobic character (high logP) of MMP inhibitors. Moreover, high hydrophobicity is responsible for unfavourable tracer biodistribution, leading to hepatobiliary clearance and high background signal.[18,19] Modification of the inhibitor lead structure to achieve analogues with logP as low as possible must be pursued, for instance by insertion of polyethylene glycol (PEG) chains of appropriate size at carefully chosen positions, as PEG is known to greatly improve water solubility with minimal effects on bioactive conformation. [19,46,47]

Our results, identifying the binding poses of arylsulfone based inhibitors on albumin binding sites, can suggest the design of new selective MMP-2 inhibitors with reduced affinity for albumin binding sites and more favourable pharmacokinetic properties to develop PET tracers with improved sensitivity and specificity for the detection of MMPs in tumors.

Materials and Methods

General procedures

Human serum albumin (lyophilized powder, essentially globulin free, ≥99%) and all other reagents were purchased from Sigma-Aldrich (catalog# A9511). Arylsulfones were synthetized according to the procedure published in ref. 22. The purity of synthesized compounds was >95% if not specified otherwise.

^{19}F-NMR studies.

^{19}F NMR spectra were acquired on a Bruker Avance III spectrometer operating at 11.7 T (corresponding to Larmor frequencies of 470 MHz and 500 MHz for ^{19}F and ^{1}H respectively), equipped with a double resonance Z-gradient 5mm BBFO probe, allowing for observation of the ^{19}F nucleus with decoupling of ^{1}H. Proton decoupled ^{19}F-NMR spectra were acquired with a 90 degree ^{19}F excitation pulse, spectral width of 220 ppm, 128K complex data points and relaxation delay of 2.5 s. The number of scans was increased from 64 (free ligand) to 16384 (protein:ligand 3:1) to get a suitable S/N all over the titration. Sample temperature was kept at 310.0 K.

For ^{19}F-NMR titration studies, a suitable amount of ligand was dissolved in 50 μL of DMSO and brought to 1.0 mL with PBS (pH 7.2, containing 10% D_2O for field/frequency lock) to obtain a final ligand concentration of 1.0 mM. Human Serum Albumin was sequentially added to 1.0 mL of ligand solution either in 50 μL aliquots of a 0.36 mM stock solution (PBS, pH 7.2) or as the solid powder up to protein to ligand:ratio of 3:1. 500 μL of the ligand/HSA mixture were transferred into a 5 mm NMR tube and a coaxial insert (sample capacity 80 μL) containing 0.3 mM trifluoroacetic acid in PBS was inserted to provide the ^{19}F-NMR chemical shift external reference (δ=0 ppm). For ^{19}F-NMR displacement experiments, 1.0 mL of PBS (pH 7.2, 10% D_2O) containing 1.0 mM of fluorinated ligand and 1.0-2.0 mM HSA was added with 20 μL of a stock solution of the displacer (either warfarin or ibuprofen) in dimethylsulfoxide. Stock solutions of the displacer were 52 or 820 mM, to obtain final concentrations of displacers of 1 mM or 16 mM, respectively. Computer aided best fit of ^{19}F-NMR titration data was done by means of Microcal Origin 8.0.

^{1}H STD-NMR.

^{1}H NMR spectra were acquired on a Agilent VNMRS NMR spectrometer operating at 14.1 T (corresponding to 600 MHz proton Larmor frequency) equipped with a 5-mm pulse field gradient (PFG) triple resonance inverse probe. Spectra were acquired using the double PFG spin echo (DPFGSE) sequence[48] for water suppression. STD-NMR spectra were acquired directly from phase

cycling and 1D ^{1}H NMR spectra were used as off-resonance reference to calculate the STD amplification factors. [30] Typical acquisition parameters for STD-NMR spectra included: spectral window 10 kHz, number of scans 2048 (128 for 1D ^{1}H spectra), spin-lock filter ($T_{1\rho}$, previously calibrated) 30 ms to remove protein resonances, acquisition time 1 s and repetition time 3 s. STD experiments were performed using a selective saturation time of 5 s at 0 ppm. Normalization for different number of acquisitions was performed as previously described.[49] Typical final concentrations for STD NMR experiments were 1.0 mM fluorinated ligand, 0.03 mM of HSA in PBS pH 7.2 containing 10% D_2O for field/frequency lock.

Computational methods

*Docking of compound **1a**.* The ligand was built using Maestro, version 9.0 (Schrödinger Inc: Portland, OR, 2009) and was subjected to a conformational search (CS) of 1000 steps, using a water environment model (generalized-Born/surface-area model) by means of Macromodel, version 9.7 (Schrödinger Inc: Portland, OR, 2009). The algorithm used was based on the Monte Carlo method with the MMFFs force field and a distance-dependent dielectric constant of 1.0. The ligand was then energy minimized using the conjugated gradient method until a convergence value of 0.05 kcal/(Å•mol) was reached, using the same force field and parameters used for the CS. Automated docking was carried out by means of the GOLD program version 5.1,[50] Autodock 4.0, [51] Fred 3.0.0,[52] and Dock6[53] in the two hypothetical binding sites. The ligand was submitted to 20 genetic algorithm runs by applying the GoldScore, ASP, GoldChemscore, GoldChemPlp fitness function and the Autodock software. Fred requires a set of input conformers for each ligand. The conformers were generated by Omega.[54] With regards to Dock, the default parameters were used, for each docking as many as 500 orientations were calculated and, of these, the best 20 grid scored were taken into consideration. For each binding site, the resulting 140 docking poses were clusterized using a threshold of 3.5 Å.

MD simulations. All simulations were performed using AMBER11. [55] MD simulations were carried out using the parm03 forcefield at 300 K. The complex was placed in a rectangular parallelepiped water box. An explicit solvent model for water, TIP3P, was used, and the complex was solvated with a 12 Å water cap. Sodium ions were added as counterions to neutralize the system. Prior to MD simulations, two steps of energy minimization were carried out. In the first stage, we kept the protein and ligand fixed with a position restraint of 100 kcal/(mol• Å^2) and we just energy minimized the positions of the water molecules. In the second stage, we applied a restraint of 30 kcal/(mol• Å^2) only on the α carbons of the receptor. The two energy minimization stages consisted of 10000 steps. The first 1000 steps were Steepest Descent, and the last 9000 were Conjugate

Gradient (CG). Molecular dynamics trajectories were run using the energy minimized structure as the input, and particle mesh Ewald electrostatics[56] and periodic boundary conditions were used in the simulation. The time step of the simulations was 2.0 fs with a cutoff of 12 Å for the non-bonded interaction. SHAKE was employed to keep all bonds involving hydrogen atoms rigid. Constant-volume periodic boundary MD was carried out for 400 ps, during which the temperature was raised from 0 to 300 K. Then 9.6 ns of constant pressure periodic boundary MD was carried out at 300 K using the Langevin thermostat to maintain constant the temperature of our system. During the whole simulation, all the α carbons of the protein were blocked with a harmonic force constant of 10 kcal/(mol• $Å^2$). General Amber force field (GAFF) parameters were assigned to the ligand, while partial charges were calculated using the AM1-BCC method as implemented in the Antechamber suite of AMBER 11.

Energy evaluation. We extracted from the last 7ns of MD of the ligand–receptor complexes, 700 snapshots (at time intervals of 10 ps) for each species (complex, receptor and ligand). The various MM-PBSA energy terms in equation 2 were computed as follows.

$$G = G_{polar} + G_{nonpolar} + E_{MM} - TS \qquad \text{eq. 2}$$

Electrostatic, van der Waals and internal energies (E_{MM}) were obtained using the SANDER module in AMBER 11. Polar energies (G_{polar}) were obtained from the PBSA module of the AMBER 11 program (using the Poisson–Boltzman method) applying dielectric constants of 1 and 80 to represent the gas and water phases, respectively. Nonpolar energies ($G_{nonpolar}$) were determined using the MOLSURF program. In order to compare the energetic interactions of the docking poses into the same binding site, we took only the first three terms of eq. 2 into account, considering the entropic value as approximately constant. Differently, to compare the binding interaction energy of compound **1a** into site-I and site-II, for the best binding pose of **1a** into the two binding sites, solute entropy was evaluated. It was estimated using the NMODE module of AMBER 11 on a total of 20 snapshots. Prior to the normal mode calculations, each species (complex, receptor, or ligand) was subjected to a CG energy minimization using a distance dependent dielectric, until a convergence of 0.0001 kcal/(mol•Å).

Acknowledgements

Economic and scientific support from Regione Piemonte (Bando CIPE 2007 “Converging Technologies”, project “BIO_THER) and from MIUR (PRIN 2010 n° 2010B5B2NL). This work

was also financially supported by FEDER and Fundação para a Ciência e a Tecnologia (Portugal) through a PhD grant to DMD (SFRH/BD/81735/2011) and Rede Nacional de RMN (REDE/1517/RMN/2005) for the acquisition of the Varian VNMRS 600 NMR spectrometer in Coimbra. This work was performed within the EU COST TD1004 Action "Theragnostics Imaging and Therapy". GD wishes to thank the students of the "Bioorganic Chemistry Lab" course for technical assistance.

Tables

Table 1. Analysis of ^{19}F-NMR titration data and binding isotherms for **1a**, **1c** and **2**.

	1a	**1c**	**2**
^{19}F-NMR Δδ, site-B	+ 1.46 ppm (690 Hz)	+ 2.50 ppm (1175 Hz)	- 1.72 ppm (810 Hz)
^{19}F-NMR Δδ, site-A	+ 0.84 ppm (394 Hz)	+ 1.13 ppm (531 Hz)	+ 0.82 ppm (384 Hz)
Association constant for type-B site (K_a^B)	1.0×10^5 M^{-1}	1.8×10^5 M^{-1}	2.6×10^5 M^{-1}
Assignment of type-B site	Sudlow site I	Sudlow site I	ambiguous
Association constant for type-A site (K_a^A)	9.0×10^3 M^{-1}	2.5×10^4 M^{-1}	3.1×10^3 M^{-1}
Number of equivalent type-A sites	2.27	1.17	4.0
Assignment of type-A site	Sudlow site II + secondary sites	Sudlow site II + secondary sites	ambiguous
Ratio K_a^A/K_a^B	0.09	0.14	0.03

Table 2. A_{STD} values and GEM (%) for the fluorinated arysulfones obtained from ^{1}H NMR STD (see supporting information for spectral data).

	Proton label	**a**	**b**	**c**	**d**	**e**	**f**	**g**	**h**	**l**
1a	A_{STD}	7.1	9.7	9.9	10.7	8.8	8.5	8.1	8.3	4.6
	GEM(%)	67.0	91.1	93.0	100	82.7	79.7	76.2	77.8	43.3
1b	A_{STD}	7.0	8.22 [a]	7.3	8.7	9.1	7.9	8.22 [a]	7.6	0
	GEM(%)	77.3	90.4 [a]	80.1	95.0	100	86.5	90.4 [a]	83.0	0
1c	A_{STD}	17.8	19.0 [b]	21.4	21.4	19.0	19.1	19.4	19.0 [b]	13.7
	GEM(%)	83.1	88.9 [b]	100	99.9	89.0	89.4	90.7	88.9 [b]	64.0
2	A_{STD}	5.7	7.5	8.4	9.4	8.4	9.7	12.1	12.7	3.5
	GEM(%)	44.8	59.1	66.0	73.9	66.2	76.1	95.1	100	27.2

[a] Overlap between the signal of H_b and H_g (see Scheme 1 for atom numbering)

[b] Overlap between the signal of H_b and H_h (see Scheme 1 for atom numbering)

Table 3. MM-PBSA results for the HSA-**1a** complexes. ΔPBSA is the sum of the electrostatic (Ele), van derWaals (VdW), polar (PB) and non-polar (PBSur) solvation free energy. Data are expressed as kcal•mol^{-1}.

Site-I					
	Ele	**VdW**	**PBsur**	**PB**	**ΔPBSA**
Pose 1	-12.7	-40.7	-3.7	36.3	-20.8
Pose 2	-26.0	-19.7	-2.3	34.0	-14.0
Pose 3	-22.2	-35.2	-3.5	40.9	-20.1
Pose 4	-2.3	-42.8	-3.6	33.3	-15.4
Pose 5	-24.2	-17.3	-1.5	32.9	-10.1
Pose 6	18.7	-41.3	-3.8	13.5	-12.8
Pose 7	-19.6	-37.3	-3.8	46.1	-14.6
Pose 8	3.4	-43.1	-3.6	27.6	-15.7
Pose 9	-38.4	-37.9	-3.8	59.0	-21.0
Pose 10	-44.7	-41.9	-4.3	53.7	-37.2
Pose 11	-4.2	-31.0	-3.3	19.2	-19.3
Pose 12	-26.8	-40.8	-4.5	55.4	-16.7
Site-II					
Pose 13	-92.3	-38.0	-3.6	111.9	-22.0
Pose 14	-69.9	-47.8	-3.4	111.6	-9.5
Pose 15	-100.3	-27.1	-2.9	113.6	-16.7
Pose 16	-61.0	-43.8	-3.4	103.8	-4.4
Pose 17	-105.8	-34.6	-3.4	124.4	-19.5
Pose 18	-146.4	-34.1	-3.0	150.0	-33.5
Pose 19	-97.3	-43.0	-3.5	124.0	-19.8
Pose 20	-125.3	-31.1	-2.8	139.3	-20.0
Pose 21	-120.7	-37.5	-3.4	140.9	-20.7
Pose 22	-131.1	-40.6	-3.4	154.5	-20.7
Pose 23	-83.8	-39.0	-3.6	107.1	-19.3
Pose 24	-48.7	-30.6	-2.9	70.5	-11.8
Pose 25	-132.9	-30.6	-2.7	145.7	-20.5
Pose 26	-47.2	-48.0	-4.3	93.9	-5.6
Pose 27	-64.9	-13.5	-1.3	75.5	-4.2

Table 4. Energy contribution to the free energy of binding (ΔG_{cal}, expressed as kcal•mol^{-1}) for compound **1a** into site-I and site-II.

	ΔE_{MM}	**ΔG_{polar}**	**$\Delta G_{nonpolar}$**	**$-T\Delta S$**	**ΔG_{cal}**
site-I	-86.6	53.7	-4.3	16.3	-20.9
site-II	-180.5	150.0	-3.0	15.8	-17.7

Schemes

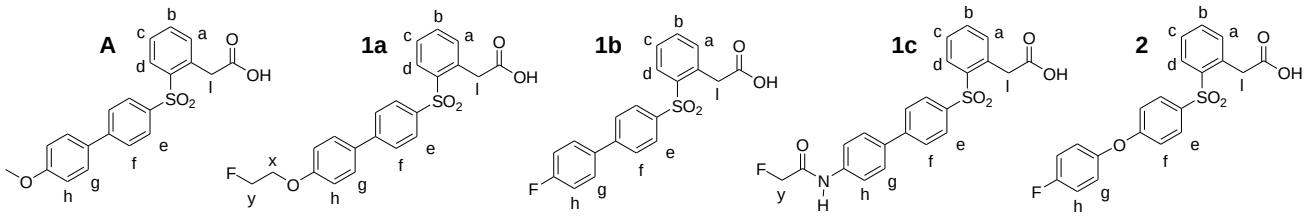

Scheme 1 − Structure of the fluorinated arylsulfones.

The synthesis and characterization of these compounds have been described in ref. 22.

Figures

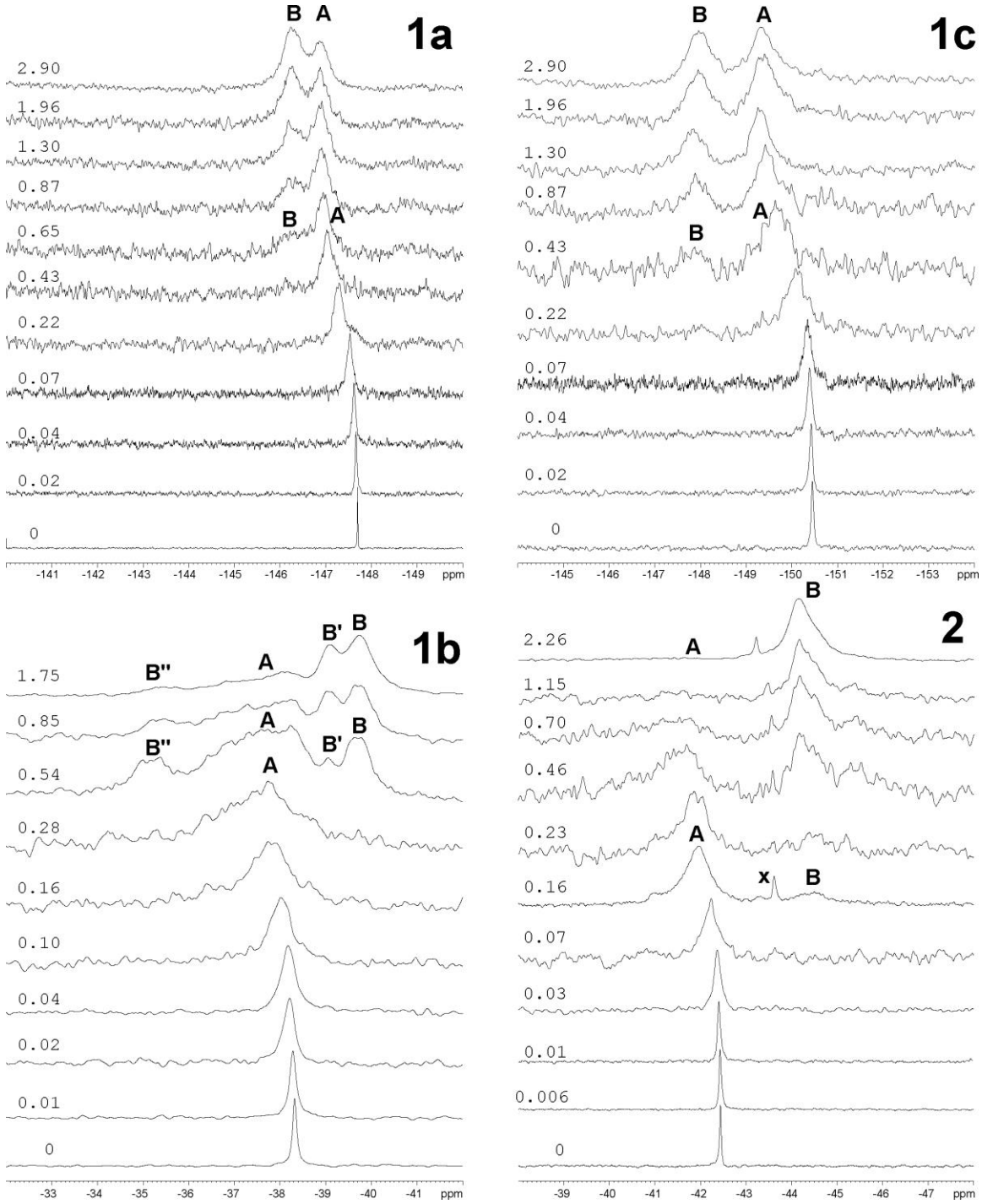

Figure 1 – ^{19}F-NMR titrations

^{19}F-NMR spectra of **1a** (1.0 mM), **1b** (1.0 mM), **1c** (1.0 mM) and **2** (1.3 mM) with increasing concentrations of HSA (PBS pH 7.2, 300 K). The final concentration of the protein in mM units is given on the left of each series of spectra. Spectra are normalized to signal intensities. ^{19}F-NMR chemical shifts are referenced to 0.3 mM TFA in D_2O (coaxial insert).

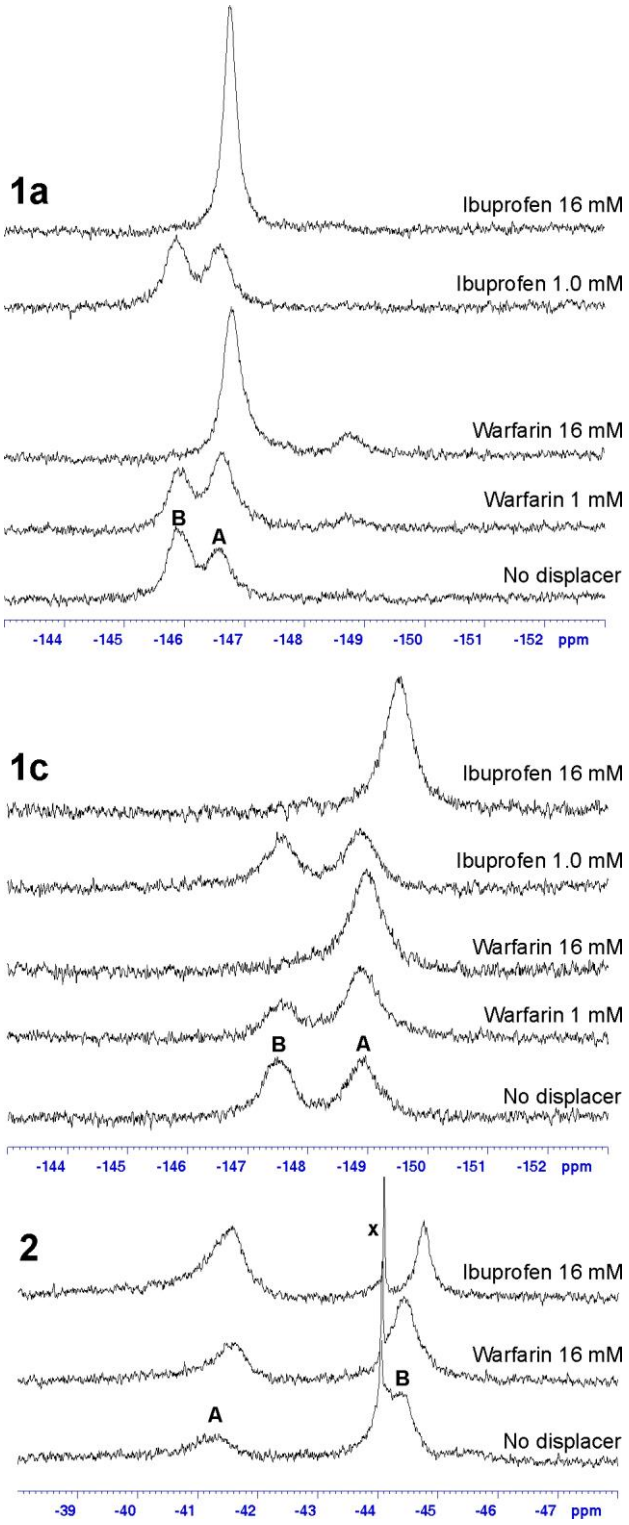

Figure 2 − Displacement of arylsulfones by ibuprofen or warfarin

^{19}F-NMR spectra of **1a**, **1c** and **2** (1.0 mM concentration) in the presence of albumin (2.0 mM for **1a**, **1c**; 1.0 mM for **2**) and a variable amount of either warfarin or ibuprofen (PBS pH 7.2, 300 K) as given in the figure legend. Type-A and type-B signals are indicated for each compound, with reference to Figure 1. "x" denotes an impurity. ^{19}F-NMR spectra were acquired with 16K scans.

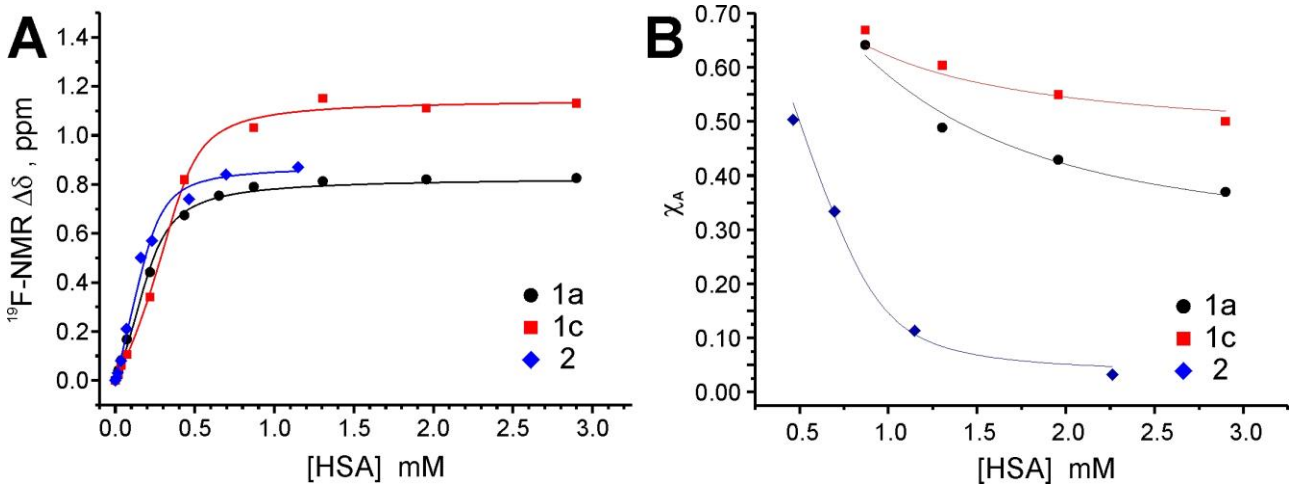

Figure 3 – ^{19}F-NMR binding isotherms

^{19}F-NMR titration of **1a** (circles), **1c** (squares) and **2** (diamond) with HSA. **A)** The ^{19}F-NMR chemical shift of signal A (Figure 1) is plotted against the total albumin concentration (HSA_T, mM). Solid lines are best fit according to the binding isotherm model accounting for the effect of high affinity binding sites on the free ligand concentration (see Supporting Information and main text for details). **B)** Plot of the molar ratio of the ligand bound at site-A (χ^A) as a function of HSA_T (only the points of the titration with high PLR have been considered). Solid lines are best fit according to the model described in the Supporting information.

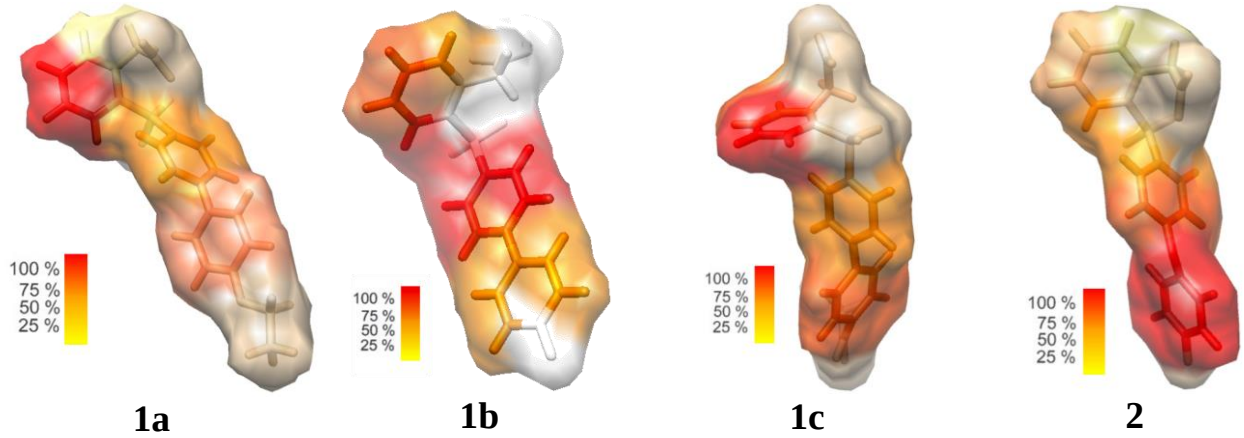

Figure 4 – Group epitope mapping from ^{1}H STD-NMR

GEM(%) mapped with colour codes onto the structure of the fluorinated arylsulfones.

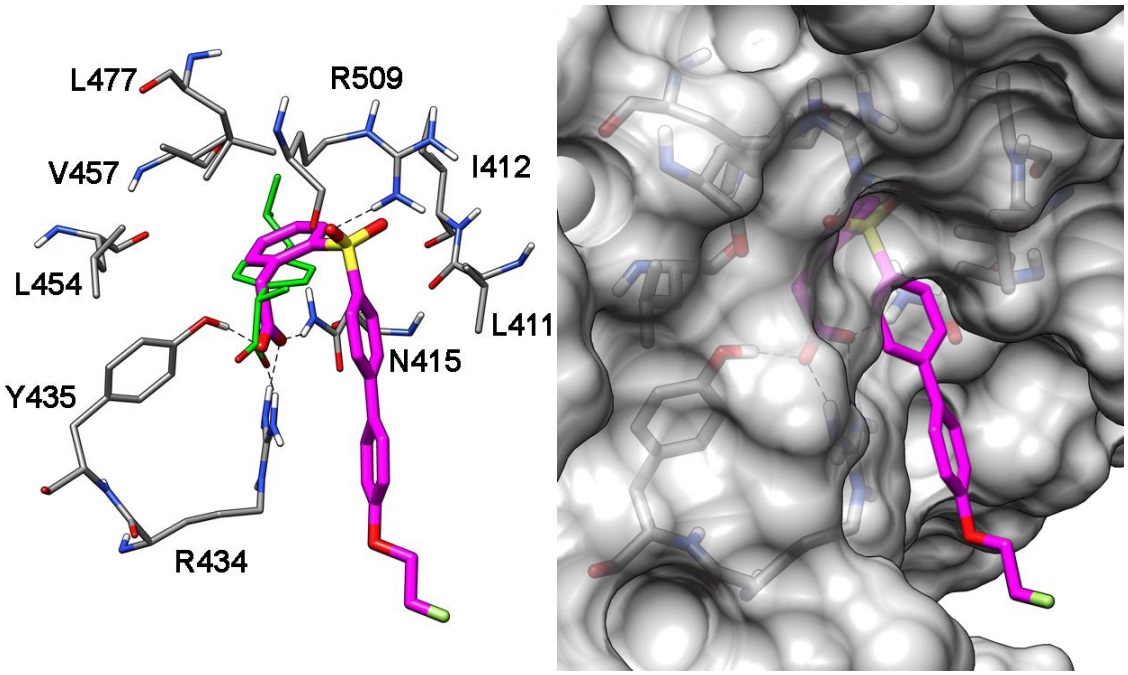

Figure 5 − Modelling of *1a* in site II.

Minimized average structures resulting from the MD simulation of the HSA-**1a** complex in Sudlow site II: main interactions and overall disposition. The crystal structure of the ibuprofen (green; PDB 2BXG) is also reported as a reference structure.

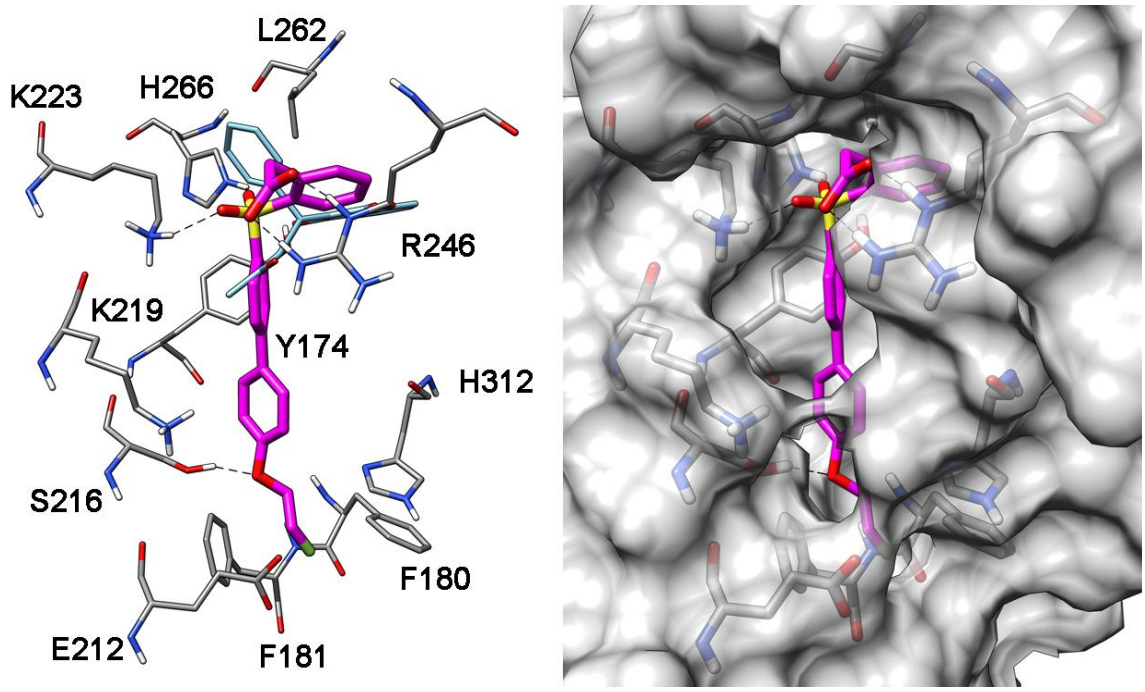

Figure 6 − Modelling of *1a* in site I.

Minimized average structures resulting from the MD simulation of the HSA-**1a** complex in Sudlow site I: main interactions and overall disposition. The crystal structure of the warfarin (cyan; PDB 2BXD) is also reported as a reference structure.

References

1 I. Massova, L.P. Kotra, R. Fridman, S. Mobashery, Matrix metalloproteinases: structures, evolution, and diversification, *FASEB J.* 12 (1998) 1075–1095.

2 H.H. Nagase, J.F. Woessner Jr., Matrix Metalloproteinases, *J. Biol. Chem*. 274 (1999) 21491–21494.

3 R. Hoekstra, F.A.L.M. Eskens, J. Verweij, Matrix Metalloproteinase Inhibitors: Current Developments and Future Perspectives, *The Oncologist* 6 (2001) 415–427.

4 W.C. Parks, C.L. Wilson, Y.S. López-Boado, Matrix metalloproteinases as modulators of inflammation and innate immunity, *Nature Rev. Immunology* 4 (2004) 617–229.

5 L.J. McCawley, L.M. Matrisian, Matrix metalloproteinases: they're not just for matrix anymore! *Current Opinion in Cell Biology* 13 (2001) 534–540.

6 M.D. Sternlicht, G. Bergers, Matrix metalloproteinases as emerging targets in anticancer therapy: status and prospects, *Emerging Ther. Targets* 4 (2000) 609–633.

7 E.I. Deryugina, J.P. Quigley, Matrix metalloproteinases and tumor metastasis, *Cancer Metastasis Rev*. 25 (2006) 9–34.

8 M. Whittaker, C.D. Floyd, P. Brown, A.J.H. Gearing, Design and therapeutic application of matrix metalloproteinase inhibitors, *Chem. Rev.* 99 (1999) 2735–2776.

9 M. Hidalgo, S.G. Eckhardt, Development of matrix metalloproteinase inhibitors in cancer therapy, *J. Natl. Cancer Inst.* 93 (2001) 178–193.

10 C. Van de Wiele, R. Oltenfreiter, Imaging probes targeting matrix metalloproteinases, *Cancer Biother. Radiopharm.* 21 (2006) 409–417.

11 B. Waschkau, A. Faust, M. Schäfers, C. Bremer, Performance of a new fluorescence-labeled MMP inhibitor to image tumor MMP activity in vivo in comparison to an MMP-activatable probe, *Contrast Media Mol. Imag.* 8 (2013) 1−11.

12 R. Lebel, B. Jastrzebska, H. Therriault, M.M. Cournoyer, J.O. McIntyre, E. Escher, W. Neugebauer, B. Paquette, M. Lepage, Novel Solubility-Switchable MRI Agent Allows the Noninvasive Detection of Matrix Metalloproteinase-2 Activity In Vivo in a Mouse Model, *Magn. Reson. Med.* 60 (2008) 1056–1065.

13 E.S. Olson, T. Jiang, T.A. Aguilera, Q.T. Nguyend, L.G. Ellies, M. Scadeng, R.Y. Tsien, Activatable cell penetrating peptides linked to nanoparticles as dual probes for in vivo fluorescence and MR imaging of proteases, *Proc. Nat. Acad. Sci.* 107 (2010) 4311–4316.

14 C.V. Gringeri, V. Menchise, S. Rizzitelli, E. Cittadino, V. Catanzaro, G. Dati, L. Chaabane, G. Digilio, S. Aime, Novel Gd(III)-based probes for MR molecular imaging of matrix metalloproteinases, *Contrast Media Mol. Imaging* 7 (2012) 175–184.

15 S. Wagner, H.-J. Breyholz, C. Höltke, A. Faust, O. Schober, M. Schäfers, K. Kopka, A new ^{18}F-labelled derivative of the MMP inhibitor CGS 27023A for PET: Radiosynthesis and initial small-animal PET studies, *Appl. Radiat. Isot.* 67 (2009) 606–610.

16 V. Hugenberg, H.-J. Breyholz, B. Riemann, S. Hermann, O. Schober, M. Schäfers, U. Gangadharmath, V. Mocharla, H. Kolb, J. Walsh, W. Zhang, K. Kopka, S. Wagner, A New Class of Highly Potent Matrix Metalloproteinase Inhibitors Based on Triazole-Substituted Hydroxamates: (Radio)Synthesis and in Vitro and First in Vivo Evaluation, *J. Med. Chem.* 55 (2012) 4714−4727.

17 U. auf dem Keller, C.L. Bellac, Y. Li, Y. Lou, P.F. Lange, R. Ting, C. Harwig, R. Kappelhoff, S. Dedhar, M.J. Adam, T.J. Ruth, F. Bénard, D.M. Perrin, C.M. Overall, Novel matrix metalloproteinase inhibitor [^{18}F]marimastat-aryltrifluoroborate as a probe for in vivo Positron Emission Tomography imaging in cancer, *Cancer Res.* 70 (2010) 7562–7569.

18 N. Matusiak, A. van Waarde, R. Bischoff, R. Oltenfreiter, C. van de Wiele, R.A.J.O. Dierckx, P.H. Elsinga, Probes for Non-invasive Matrix Metalloproteinase-targeted Imaging with PET and SPECT, *Curr. Pharm. Design* 19 (2013) 4647–4672.

19 H.-J. Breyholz, S. Wagner, A. Faust, B. Riemann, C. Höltke, S. Hermann, O. Schober, M. Schäfers, K. Kopka, Radiofluorinated pyrimidine-2,4,6-triones as molecular probes for noninvasive MMP-targeted imaging, *ChemMedChem* 5 (2010) 777–789.

20 S. Furomoto, K. Takashima, K. Kubota, T. Ido, R. Iwata, H. Fukuda, Tumor detection using ^{18}F-labeled matrix metalloproteinase-2 inhibitor. *Nucl. Med. Biol.* 30 (2003) 119–125.

21 E. Nuti, L. Panelli, F. Casalini, S.I. Avramova, E. Orlandini, S. Santamaria, S. Nencetti, T. Tuccinardi, A. Martinelli, G. Cercignani, N. D'Amelio, A. Maiocchi, F. Uggeri, A. Rossello, Design, synthesis, biological evaluation, and NMR studies of a new series of arylsulfones as selective and potent matrix metalloproteinase-12 inhibitors, *J. Med. Chem.* 52 (2009) 6347–6361.

22 F. Casalini, L. Fugazza, G. Esposito, C. Cabella, C. Brioschi, A. Cordaro, L. D'Angeli, A. Bartoli, A.M. Filannino, C.V. Gringeri, D.L. Longo, V. Muzio, E. Nuti, E. Orlandini, G. Figlia, A. Quattrini, L. Tei, G. Digilio, A. Rossello, A. Maiocchi, Synthesis and Preliminary Evaluation in Tumor Bearing Mice of New [^{18}F]-labelled Arylsulfone Matrix Metalloproteinase Inhibitors as Tracers for Positron Emission Tomography, *J. Med. Chem.* 56 (2013) 2676−2689.

23 J. Ghuman, P.A. Zunszain, I. Petitpas, A.A. Bhattacharya, M. Otagiri, S. Curry, Structural basis of the drug binding specificity of Human Serum Albumin, *J. Mol. Biol.* 353 (2005) 38−52.

24 H. Mao, P.J. Hajduck, R. Craig, R. Bell, T. Borre, S.W. Fesik, Rational design of diflunisal analogues with reduced affinity for human serum albumin, *J. Am. Chem. Soc.* 43 (2001) 10429−10435.

25 T. Peters Jr., All about albumin: Biochemistry, Genetics and Medical Applications, Academic Press, Orlando FL, 1996.

26 G. Sudlow, D.J. Birkett, D.N. Wade, The Characterization of Two Specific Drug Binding Sites on Human Serum Albumin, *Mol. Pharmacol.* 11 (1975) 824–832.

27 U. Krag-Hansen, V.T.G. Chuang, M. Otagiri, Practical aspects of the ligand-binding and enzymatic properties of human serum albumin, *Biol. Pharm. Bull.* 25 (2002) 695–704.

28 F.P. Nicoletti, B.D. Howes, M. Fittipaldi, G. Fanali, M. Fasano, P. Ascenzi, G. Smulevich, Ibuprofen induces an allosteric conformational transition in the heme complex of human serum albumin with significant effects on heme ligation, *J. Am. Chem. Soc.* 130 (2008) 11677–11688.

29 S. Aime, G. Digilio, E. Bruno, V. Mainero, S. Baroni, M. Fasano, Modulation of the antioxidant activity of HO$^{\bullet}$ scavengers by albumin binding: a ^{19}F-NMR study. *Biochim. Biophys. Res. Commun.* 307 (2003) 962–966.

30 M. Mayer, B. Meyer, Characterization of Ligand Binding by Saturation Transfer Difference NMR Spectroscopy, *Angew. Chem. Int. Ed.* 38 (1999) 1784–1788.

31 M. Mayer, B. Meyer, Group Epitope Mapping by Saturation Transfer Difference NMR To Identify Segments of a Ligand in Direct Contact with a Protein Receptor, *J. Am. Chem. Soc.* 123 (2001) 6108–6117.

32 P.A. Kollman, I. Massova, C. Reyes, B. Kuhn, S. Huo, L. Chong, M. Lee, T. Lee, Y. Duan, W. Wang, O. Donini, P. Cieplak, J. Srinivasan, D.A. Case, T.E. Cheatham, Calculating structures and free energies of complex molecules: combining molecular mechanics and continuum models, *Acc. Chem. Res.* 33 (2000) 889–897.

33 T. Tuccinardi, S. Bertini, A. Martinelli, F. Minutolo, G. Ortore, G. Placanica, G. Prota, S. Rapposelli, K.E. Carlson, J.A. Katzenellenbogen, M. Macchia, Synthesis of anthranylaldoxime derivatives as estrogen receptor ligands and computational prediction of binding modes, *J. Med. Chem.* 49 (2006) 5001–5012.

34 T. Tuccinardi, F. Manetti, S. Schenone, A. Martinelli, M. Botta, Construction and validation of a RET TK catalytic domain by homology modelling, *J. Chem. Inf. Model.* 47 (2007) 644–655.

35 B. Cao, S. Endsley, N.H. Andersen, ^{19}F NMR studies of triptophan/serum albumin binding, *Bioorg. Med. Chem.* 11 (2003) 69−75.

36 B.G. Jenkins, R.B. Lauffer, Detection of site-specific binding and co-binding of ligands to human serum albumin, *Mol. Pharmacol.* 37 (1990) 111–118.

37 J.T. Gerig, J.C. Klinkenborg, Binding of 5-fluoro-L-triptophan to human serum albumin, *J. Am. Chem. Soc.* 102 (1980) 4267–4268.

38 M.S. Dennis, H. Jin, D. Dugger, R. Yang, L. McFarland, A. Ogasawara, S. Williams, M.J. Cole, S. Ross, R. Schwall, Imaging Tumors with an Albumin-Binding Fab, a Novel Tumor-Targeting Agent, *Cancer Res*. 67 (2007) 254–61.

39 H. Nakagawa, D.R. Groothuis, E.S. Owens, J.D. Fenstermacher, C.S. Patlak, R.G. Blasberg, Dexamethasone Effects on [^{125}I]Albumin Distribution in Experimental RG-2 Gliomas and Adjacent Brain, *J. Cereb. Blood Flow Metab.* 7 (1987) 687–701.

40 A.P. Pathak, D. Artemov, B.D. Ward, D.G. Jackson, M. Neeman, Z. Bhujwalla, Characterizing Extravascular Fluid Transport of Macromolecules in the Tumor Interstitium by Magnetic Resonance Imaging. *Cancer Res.* 65 (2005) 1425–1432.

41 W. Eckelman, The application of receptor theory to receptor-binding and enzyme-binding oncologic radiopharmaceuticals, *Nucl. Med. Biol.* 21 (1994) 759–769.

42 R. Oltenfreiter, L. Stùaelens, A. Lejeune, F. Dumont, F. Frankenne, J.-M. Foidart, G. Slegers, New radioiodinated carboxylic and hydroxamic matrix metalloproteinase inhibitor tracers as potential tumor imaging agents, *Nucl. Med. Biol.* 31 (2004) 459–468.

43 J. Cortes, C. Saura, Nanoparticle albumin-bound (nab^{TM})-paclitaxel : improving efficacy and tolerability by targeted drug delivery in metastatic breast cancer, *Eur. J. Cancer Supplements* 8 (2010), 1–10.

44 K. Motamed, SPARC (osteonectin/BM-40), *Int. J. Biochem Cell Biol.* 31 (1999) 1363–1366.

45 C.J. Clark, E.H. Sage, A Prototypic Matricellular Protein in the Tumor Microenvironment–Where There's SPARC, There's Fire, *J. Cell. Biochem.* 104 (2008) 721–732.

46 A. Faust, B. Waschkau, J. Waldeck, C. Holtke, H. J. Breyholz, S. Wagner, K. Kopka, W. Heindel, M. Schäfers, C. Bremer, Synthesis and Evaluation of a Novel Fluorescent Photoprobe for Imaging Matrix Metalloproteinases, *Bioconjugate Chem.* 19 (2008) 1001–1008.

47 G. Digilio, L. Barbero, C. Bracco, D. Corpillo, P. Esposito, G. Piquet, S. Traversa, S. Aime, NMR Structure of Two Novel Polyethylene Glycol Conjugates of the Human Growth Hormone-Releasing Factor, hGRF(1-29)-NH2, *J. Am. Chem. Soc.* 125 (2003) 3458–3470.

48 T.-L. Hwang, A.J. Shaka, Suppression that works: excitation sculpting using arbitrary waveforms and pulse field gradients, *J. Magn. Reson.* 112 (1995) 275–279.

49 J.M.C. Teixeira, D.M. Dias, F.J. Cañada, J.A. Martins, J.P. André, J. Jiménez-Barbero, C.F.G.C. Geraldes, The interaction of La^{3+} complexes of DOTA/DTPA glycoconjugates with the RCA(120) lectin: a saturation transfer difference NMR spectroscopic study, *J. Biol. Inorg. Chem.* 16 (2011) 725–734.

50 M.L. Verdonk, J.C. Cole, M.J. Hartshorn, C.W. Murray, R.D. Taylor, Improved protein-ligand docking using GOLD, *Proteins* 52 (2003) 609–623.

51 G.M. Morris, R. Huey, W. Lindstrom, M.F. Sanner, R.K. Belew, D.S. Goodsell, A.J. Olson, AutoDock4 and AutoDockTools4: Automated docking with selective receptor flexibility, *J. Comput. Chem.* 30 (2009) 2785–2791.

52 FRED, version 3.0.0. In OpenEye Scientific Software, Inc., Santa Fe, NM, USA, www.eyesopen.com, 2013.

53 DOCK, version 6.0. In Molecular Design Institute, University of California: San Francisco, CA, 1998.

54 OMEGA, version 2.4.6. In OpenEye Scientific Software, Inc., Santa Fe, NM, USA, www.eyesopen.com, 2013.

55 D.A. Case, T.A. Darden, T. E. Cheatham, III, C.L. Simmerling, J. Wang, R.E. Duke, R. Luo, R.C. Walker, W. Zhang, K.M. Merz, B. Roberts, B. Wang, S. Hayik, A. Roitberg, G. Seabra, I. Kolossváry, K.F. Wong, F. Paesani, J. Vanicek, J. Liu, X. Wu, S.R. Brozell, T. Steinbrecher, H. Gohlke, Q. Cai, X. Ye, J. Wang, M.-J. Hsieh, G. Cui, D.R. Roe, D.H. Mathews, M.G. Seetin, C. Sagui, V. Babin, T. Luchko, S. Gusarov, A. Kovalenko, P.A. Kollman, AMBER, version 11, (2010), University of California, San Francisco, CA.

56 U. Essmann, L. Perera, M.L. Berkowitz, T.A. Darden, H. Lee, L.G. Pedersen, A smooth particle mesh Ewald method, *J. Chem. Phys.* 103 (1995) 8577–8594.